PAPER

Characterization of dielectric function for metallic thin films based on ellipsometric parameters and reflectivity

IOP Publishing Physica Scripta
Phys. Scr. 94 (2019) 085802 (15pp) https://doi.org/10.1088/1402-4896/ab1606

Characterization of dielectric function for metallic thin films based on ellipsometric parameters and reflectivity

Jiamin Liu, Jianbin Lin, Hao Jiang[1], Honggang Gu, Xiuguo Chen, Chuanwei Zhang, Guanglan Liao and Shiyuan Liu[1]

State Key Laboratory of Digital Manufacturing Equipment and Technology, Huazhong University of Science and Technology, Wuhan 430074, People's Republic of China

E-mail: hjiang@hust.edu.cn and shyliu@hust.edu.cn

Received 11 December 2018, revised 28 March 2019
Accepted for publication 4 April 2019
Published 29 April 2019

Abstract

A synergic analysis method based on ellipsometric parameters and reflectivity is proposed to simultaneously determine the thickness and the thickness-dependent dielectric functions of metallic thin films on the opaque substrate. Both the ellipsometric parameters and reflectivity are measured by one spectroscopic ellipsometer. The proposed method consists of a point-by-point synergic regression analysis on the ellipsometric parameters and the reflectivity as well as an oscillator-parametrization regression analysis on the ellipsometric parameters. The oscillator-parametrization model is composed of the Drude oscillator, two TaucLorentz oscillators and a Lorentz oscillator, which describe the intraband, the interband and the plasmon contributions to the dielectric functions, respectively. Practical measurement experiments on a series of Cu thin films deposited on Si substrates have been carried out for demonstration, in which a broad spectral range of 0.73–4.96 eV has been covered. The relative deviations between the thicknesses reported by our method and reported by Atomic Force Microscopy and Transmission Electron Microscopy are less than 3.5%, which verifies the validity and the accuracy of the proposed method. Meanwhile, the results of oscillator-parametrization regression analysis indicate that both the real part ε_1 and the imaginary part ε_2 of the dielectric functions decrease with the increasing Cu film thickness in the range of 6.8–12.9 nm. Besides, the fitting results also exhibits that both the plasma energy and the Drude relaxation time increase monotonically with the thickness increasing, in which the increasing of Drude relaxation time can be attributed to the increasing of surface scattering time.

Keywords: ellipsometric parameters, reflectivity, dielectric function, thickness dependency, metallic thin film

(Some figures may appear in colour only in the online journal)

1. Introduction

It has been widely reported that the dielectric functions of the metallic thin films are significantly different to those of the corresponding bulk materials due to the downscaling [1–3]. The metallic thin films, such as noble metal films [4] and metal alloy films [5], have attracted plenty of research interests and been comprehensively applied in many fields such as plasmonic materials [6], semiconductor devices [7], magnetic DRAM [8], optical meta-materials [9] and optical coating stacks [10], etc. Since the performances of these films heavily depend on their thicknesses and dielectric functions, it is highly desirable to precisely characterize these parameters of such metallic thin films for better applications.

Due to the advantages, such as high sensitivity and non-destructive, spectroscopic ellipsometer (SE) has been practically

[1] Authors to whom any correspondence should be addressed.

used as a standard metrology tool for the optical constants and thin film thickness [11–13]. However, there exists a strong correlation between the thickness and the dielectric function of the metallic thin film [14], which acts as an inevitable barrier to simultaneously determine the thickness and the dielectric function for such a thin film sample in one trial. In the past decades, several improvements have been proposed to decouple such a correlation and consequently ensure the accurate measurement of the metallic thin films [15]. These improvements, including the multiple-angle measurement [16], the interference enhancement [17], the dielectric function parametrization modeling [18] and the method combining SE and transmittance [19], have been successfully applied in the measurements of the metallic thin films of various types. However, these methods also have exhibited specific limitations. For instance, the effective implementation of the multiple-angle measurement relies on a prior condition that new information about the sample can be acquired by varying the incident angles [20]. This prior condition is rather harsh for lots of ultrathin metal films and difficult to be satisfied. Interference enhancement has been demonstrated and applied on measuring the thickness and the dielectric function of CoFeB [21]. However, an additional manufacturing process needs to be introduced to add a rather thicker transparent film below the metallic layer, which raises the cost and the complexity of the experiments. Utilizing some dispersion equations to describe the dielectric functions of metallic thin films [22] is an effective strategy to significantly reduce the total number of unknown parameters. But unfortunately, identifying an accurate dispersion model for the metallic film usually needs too much prior knowledge. And it is extremely difficult to obtain the unique value of thickness through simultaneous fitting the thickness and dielectric function based on the dispersion equations, due to the strong coupling effect between the thickness and dispersion model, when the film is ultrathin. By additionally introducing the transmittance measurement in SE metrology, the achieved information about the sample has been remarkably enhanced [23], and consequently, a unique solution set of the thickness and the dielectric function can be possibly found via the regression analysis of ellipsometric parameters and transmittance [24, 25]. Slightly differently, the method combining *in situ* transmitted SE and transmission intensity has also been reported to simultaneously determine the thickness and the dielectric function of metallic thin films such as Al, Co, Mo and Ti films [26]. However, the metallic thin films should be deposited on transparent substrates due to the measurement of transmittance, which limits the application. Although reflected intensity has been reported having similar sensitivity as transmitted intensity using regression based multi-angle measurements [15], due to the noises in the intensity data as well as the possible inappropriate angle combination selection, abnormal oscillations in the resulted dielectric function and insufficient information may degrade both sensitivity and robustness. In the worst cases, unique solution might be difficult to be achieved. Besides, the method combining the total internal reflection ellipsometry with standard ellipsometry and reflectometry has been adopted to measure the dielectric function and the thickness of Ag films with the enhanced sensitivity to the measurand [27–29]. However, an additional BK7 prism should be added on the transparent substrate, which increases the complexity of the experiment and the corresponding forward optical model.

In this paper, a synergic analysis method based on ellipsometric parameters and reflectivity has been proposed, which enables the simultaneous determination of the thickness and the dielectric function for the metallic thin film. Both the ellipsometric parameters, including the amplitude ratio and the phase difference between p- and s-components, and the reflectivity are acquired using one ellipsometer. With the establishment of the forward optical model corresponding to the metallic thin film, the accurate thickness and a rough dielectric function can be extracted using the point-by-point synergic regression analysis of the ellipsometric parameters and the reflectivity. Then, with a Drude-Dual-TaucLorentz-Lorentz dispersion model we proposed and the achieved thickness, the accurate dielectric function will be obtained by applying the oscillator-parametrization regression analysis on the ellipsometric parameters. Practical experiments on measuring a series of Cu thin films deposited on Si substrates have been sequentially carried out for demonstration. The results clearly show the coupling effect between the thickness and dielectric function of these samples. And by comparing with the thicknesses reported by Atomic Force Microscopy (AFM) and Transmission Electron Microscopy (TEM), the validity and the accuracy of the proposed method have been verified. Furthermore, the thickness-dependent dielectric function, the plasma energy, the Drude relaxation time, and the surface relaxation time of the Cu thin films, have been discussed as well.

2. Method

Essentially, the thickness and the dielectric function are obtained by fitting the measured ellipsometric parameters and reflectivity with the calculated ones using a forward optical model. Accordingly, the method consists of two steps: one is the acquisition of the ellipsometric parameters and the reflectivity using an ellipsometer, and the other is the synergic regression analysis strategy based on the forward optical model.

2.1. Metrology of ellipsometric parameters and reflectivity

If the metallic thin films are isotropic, an arbitrary set of measured ellipsometric parameters can be expressed as equation (1),

$$\rho_{\mathrm{meas}} = \frac{r_{\mathrm{p}}}{r_{\mathrm{s}}} = \frac{|r_{\mathrm{p}}|}{|r_{\mathrm{s}}|}\exp[\mathrm{i}(\delta_{\mathrm{p}} - \delta_{\mathrm{s}})] = \tan\psi_{\mathrm{meas}} \cdot \exp(\mathrm{i}\Delta_{\mathrm{meas}}), \tag{1}$$

where ρ_{meas} is the ratio of reflection coefficients r_{p} and r_{s} respectively for p- and s-components. $|r_{\mathrm{p}}|$ and $|r_{\mathrm{s}}|$ are the amplitude of r_{p} and r_{s}, respectively. δ_{p} and δ_{s} represent the phase-shifts of p- and s-components, respectively [30–32]. Both ψ_{meas} and Δ_{meas} are the measured ellipsometric parameters.

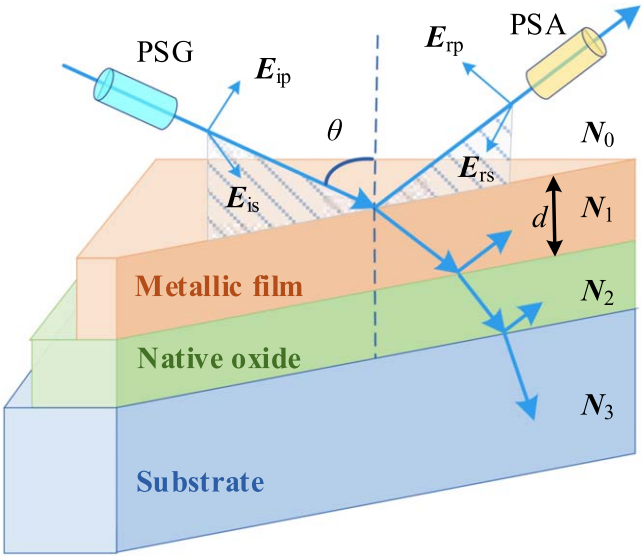

Figure 1. The schematic of the optical paths of the probing light and the layered structure model of the metallic thin film. N_1 and d are the optical constant and thickness of metallic film. N_0, N_2 and N_3 are the optical constants of air, the intermediate layer and the substrate, respectively. θ is the incident angles. PSG and PSA represent the polarization state generator and the polarization state analyzer, respectively. E_{ip} and E_{is} are the polarization components of the incident beam. E_{rp} and E_{rs} are the polarization components of the reflected beam.

In contrast with the measurement process of ellipsometric parameters, each reflectivity measurement of the metallic thin film consists of the intensity measurements on a reference sample and the metallic thin film under specific incident angles. Usually, the standard SiO_2 film on a Si substrate with the nominal thickness of 25 nm is selected as the reference sample. Accordingly, the reflectivity R_{meas} measured by the SE can be calculated using

$$R_{meas} = \frac{I_S - I_{DC}}{I_R - I_{DC}} R_R, \tag{2}$$

where I_S and I_R are the measured light intensities for the films and the reference sample, respectively. I_{DC} represents the direct-current component. R_R is the reflectivity of the reference sample contained in the library of the software for SE, which can be calculated from the forward optical model.

2.2. Data analysis

The optical responses of the ideal metallic thin films to the probing light, such as ψ_{meas}, Δ_{meas} and R_{meas}, can be approximated by a forward optical model employing an ambient/surface layer/metallic thin film/intermediate layer/substrate structure as shown in figure 1. An intermediate layer has been inserted between the substrate and the metallic thin film to be characterized, which is used to consider the possible effects of the roughness and native oxide layer on the Si substrate. By parametrizing each layer with the corresponding complex dielectric function and the thickness, the interaction between the probing light and the sample can be described based on the Fresnel optical interference [33]. At the interesting metallic film thickness, the anomalous skin effect possibly has influence on the reflection coefficients [34, 35]. Since the purpose of the proposed method is decoupling the strong correlations between thickness and dielectric functions of metallic films and considering the successful application of Fresnel optical interference model on similar objects [2–4, 8, 12–19], we adopted Fresnel optical interference model for the calculation of reflection coefficients and only considered the influence of such effect on the surface relaxation time. Correspondingly, the ellipsometric parameters ψ and Δ can be defined as the functions of the parameters of the analyzed metallic thin film layer,

$$\rho_{calc} = \tan(\psi_{calc}) \cdot \exp(i\Delta_{calc}) = f(\varepsilon_1, \varepsilon_2, d), \tag{3}$$

where ε_1, ε_2 and d represent the real part and the imaginary part of dielectric function and the thickness of the interested metallic thin film layer, respectively. $f(\varepsilon_1, \varepsilon_2, d)$ is the function based on the forward optical model. Both ψ_{calc} and Δ_{calc} are the calculated ellipsometric parameters. ρ_{calc} is the ratio of calculated reflection coefficients of p- and s-components.

The reflectivity R_{calc} of the metallic thin films under an oblique irradiating polarized beam can be given by,

$$R_{calc} = \frac{I_r}{I_i} = \frac{I_{rp} + I_{rs}}{I_{ip} + I_{is}} = \frac{R_p I_{ip} + R_s I_{is}}{I_{ip} + I_{is}} = \frac{I_{is} \cdot (R_p \eta_{ps} + R_s)}{I_{is} \cdot (\eta_{ps} + 1)} = \frac{R_p \eta_{ps} + R_s}{1 + \eta_{ps}}, \tag{4}$$

where I_r and I_i are the intensities of the reflected and incident light, respectively. I_{ip} and I_{is} are the intensities of p- and s-components of the incident light, respectively. I_{rp} and I_{rs} stand for the intensities of p- and s-components of the reflected light, respectively. $R_p = |r_p|^2$ and $R_s = |r_s|^2$ represent the reflectivities of p- and s-components, respectively. $\eta_{ps} = I_{ip}/I_{is}$ is the intensity ratio of p- and s-components of the incident light. η_{ps} is very close to unity due to the averaging effect of the polarization modulation in a SE, whose exact value can be obtained through the calibration of SE with the standard SiO_2 film. With the usage of the calibration value of η_{ps}, R_{calc} can be calculated from the forward optical model based on the Fresnel optical interference.

Considering that ψ_{meas}, Δ_{meas} and R_{meas} are transcendental functions of the thickness and the dielectric function of the metallic thin film, we introduce a weighted least-squares regression analysis to reconstruct the thickness and the dielectric function [36]. Meanwhile, due to the strong correlation between the thickness and the dielectric function, the above regression analysis is further divided into two steps, i.e. a point-by-point fitting and a whole-spectrum fitting, as shown in figure 2. The point-by-point fitting process enables the global search of the thickness and the decoupling of the thickness and the dielectric functions. Specifically, during the point-by-point synergic fitting, the thickness is firstly traversed in a pre-estimated range $[d_1\ d_2]$ with an increment Δd. At each traversed value of thickness, the ψ_{meas}, Δ_{meas} and R_{meas} are simultaneously fitted by adapting the ε_1 and ε_2 at

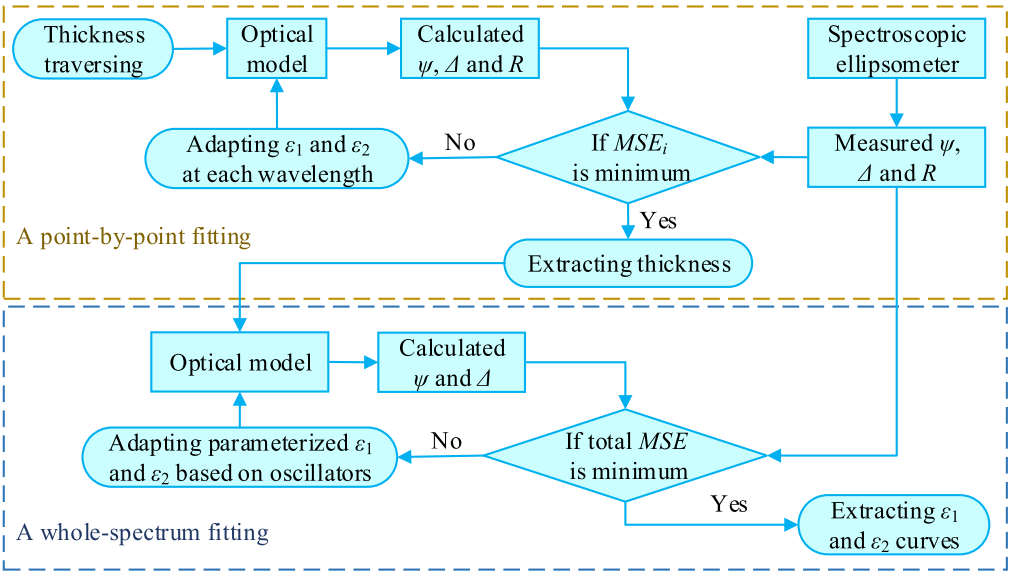

Figure 2. The analytic flow chart of the proposed method.

each wavelength, and correspondingly, the mean square error (MSE) at each wavelength will be calculated based on the merit function of fitting defined as equation (5). By summing the MSE at each wavelength, the total MSE corresponding to each traversed thickness d_i can be obtained. When the minimum of the total MSE is achieved, the corresponding approximate thickness d_m of the metallic thin film can also be determined. Then, the above point-by-point synergic fitting will be carried out for the second time in a smaller pre-estimated interval $[d_3\ d_4]$ containing d_m with a refined increment δd. Similarly, the extracted thickness d of the metallic film can finally be determined when the minimum of the total MSE is achieved.

$$[\varepsilon_{1,i},\ \varepsilon_{2,i},\ d] = \underset{\Omega}{\operatorname{argmin}}\left\{\sum[\mathrm{MSE}_i]\right\} = \underset{\Omega}{\operatorname{argmin}}\left\{\sum_{\lambda_i}[(\psi_i^{\mathrm{meas}} - \psi_i^{\mathrm{calc}})^2 + (\Delta_i^{\mathrm{meas}} - \Delta_i^{\mathrm{calc}})^2 + (R_i^{\mathrm{meas}} - R_i^{\mathrm{calc}})^2]\right\} \tag{5}$$

where d represents the traversed thickness. $\varepsilon_{1,i}$ and $\varepsilon_{2,i}$ are the extracted real part and imaginary part of dielectric function at the ith wavelength, respectively. MSE_i is the MSE at the ith wavelength. $\psi_{\mathrm{meas}i}$, $\Delta_{\mathrm{meas}i}$ and $\mathrm{R}_{\mathrm{meas}i}$ are the measured ellipsometric parameters and reflectivity at the ith wavelength, respectively. And $\psi_{\mathrm{calc}i}$, $\Delta_{\mathrm{calc}i}$ and $R_{\mathrm{calc}i}$ stand for the calculated ellipsometric parameters and reflectivity at the ith wavelength from the forward optical model, respectively.

Since the accuracy of ε_1 and ε_2 extracted from the point-by-point fitting will be seriously degraded by the noises in the measured data, we have proposed an oscillator-parametrized model to describe the dielectric function of the metallic thin film for the whole-spectrum fitting of ψ_{meas} and Δ_{meas}. In the model, the optical constants of the intermediate layer and Si substrate are quoted from [20], and the thickness of the intermediate layer will be set as the extracted value from the ellipsometric measurement of original Si substrate. Supposing a Cu thin film deposited on a Si substrate is the object of study, the corresponding dielectric function can be described by the superposition of a Drude oscillator, two TaucLorentz oscillators and a Lorentz oscillator, shown as equation (6),

$$\varepsilon = \varepsilon_{\mathrm{Drude}} + \sum_{i=1}^{2}\varepsilon_{\mathrm{TaucLorentz},i} + \varepsilon_{\mathrm{Lorentz}}, \tag{6}$$

where $\varepsilon_{\mathrm{Drude}}$, $\varepsilon_{\mathrm{Lorentz}}$ and $\varepsilon_{\mathrm{TaucLorentz}}$ represent the Drude oscillator, the Lorentz oscillator and the TaucLorentz oscillator, respectively.

The Drude oscillator $\varepsilon_{\mathrm{Drude}}$ is dominated by the intraband transitions of the free electrons in the metallic thin films [37], which is used to describe the dielectric function of Cu film in the spectrum from the near-infrared to the visible light. The corresponding equation can be expresses as,

$$\varepsilon_{\mathrm{Drude}} = \varepsilon_\infty - \frac{E_{\mathrm{p}}^2}{En^2 - \mathrm{i}\Gamma_{\mathrm{Drude}}En}, \tag{7.1}$$

where ε_∞ is the high frequency dielectric constant due to the effect of interband transition at much higher energy. En is the photon energy in the range of 0.73–4.96 eV, which determined by the spectrum of ellipsometer. $E_{\mathrm{p}} = \hbar\omega_{\mathrm{p}}$ is the energy corresponding to the bulk plasma frequency ω_{p}. $\hbar$ is

reducible Planck constant. $\Gamma_{\text{Drude}} = \hbar/\tau_{\text{Drude}}$ represents the electron relaxation energy corresponding to the Drude relaxation time τ_{Drude}. The plasma frequency can be expressed as a function of the conduction electron density N_e and the electron effective mass m^* [38], shown as equation (7.2)

$$\omega_p^2 = \frac{N_e e^2}{m^* \cdot \varepsilon_0}, \tag{7.2}$$

where ε_0 is the vacuum permittivity, e is the charge of electron.

The Drude relaxation time τ_{Drude} describes the scattering mechanism of the free electrons in the metallic thin films, including the bulk scattering effect and the surface scattering effect [39]. The former is induced by the collisions between electrons and phonons, the collisions between electrons and electrons, and the collisions between electrons and the grain boundaries [40]. The latter arises are caused by the diffuse scattering of electrons at the surface of Cu film, which leads to the strong absorption of noble metals in the near-infrared band [39]. The corresponding equation are shown as equation (7.3),

$$\frac{1}{\tau_{\text{Drude}}} = \frac{1}{\tau_{\text{bulk}}} + \frac{1}{\tau_{\text{surface}}} = \frac{1}{\tau_{ep}} + \frac{1}{\tau_{ee}} + \frac{1}{\tau_{eb}} + \frac{1}{\tau_{\text{surface}}}, \tag{7.3}$$

where τ_{bulk} and τ_{surface} are the bulk relaxation time and the surface relaxation time, respectively. τ_{ep}, τ_{ee} and τ_{eb} represent the electron-phonon relaxation time, the electron–electron relaxation time and the electron-grain-boundary relaxation time, respectively.

In the studied spectrum from the near-infrared to the visible light, the inverse time of flight of Fermi electron in the studied Cu film becomes comparable with or slightly less than the frequency of electromagnetic wave, the anomalous skin effect should be carefully considered in the surface relaxation time τ_{surface} [41]. Correspondingly, the surface relaxation time can be shown as,

$$\frac{1}{\tau_{\text{surface}}} = \frac{3}{8}\left(\frac{v_F}{c}\right)\omega_p = \frac{3}{8}\left(\frac{v_F}{c}\right) \cdot \sqrt{\frac{N_e^2}{m^* \cdot \varepsilon_0}}, \tag{7.4}$$

where v_F and c are the Fermi velocity and the light velocity, respectively.

The Lorentz oscillator $\varepsilon_{\text{Lorentz}}$ describes the plasmons behavior at near-infrared spectrum or higher [32, 42]. The corresponding equation can be expressed as,

$$\varepsilon_{\text{Lorentz}} = \frac{A_{\text{Lorentz}} \cdot E_{\text{Lorentz}}^2}{(E_{\text{Lorentz}}^2 - En^2) - \mathrm{i}\Gamma_{\text{Lorentz}} En}, \tag{8}$$

where E_{Lorentz}, A_{Lorentz} and Γ_{Lorentz} stand for the plasmon resonance energy, the resonance strength and the broadening parameter, respectively.

Usually, the interband transition contribution to the dielectric function of noble metals can be roughly described by combining several Lorentz oscillators [43] or several critical point oscillators [44]. However, the former has not sufficiently considered the asymmetric line shape of the absorption peaks in the interband transition spectra, and the latter possesses an even worse fitting result in the near-infrared spectra for ε of bulk Cu [45]. Here, we introduce a dual-TaucLorentz oscillator model to describe the dielectric responses of Cu films in the interband transition region [46] as,

$$\varepsilon_{2,\text{TaucLorentz},i} = \begin{cases} \dfrac{1}{En} \times \dfrac{A_i \times E_i \times C_i \times (En - Eg_i)^2}{(En^2 - E_i^2)^2 + C_i^2 \times E_i^2} En > Eg_i \; i = 1, 2. \\ 0 En \leqslant Eg_i \end{cases} \tag{9}$$

$$\varepsilon_{1,\text{TaucLorentz},i} = \frac{2}{\pi} \mathrm{P} \int_{Eg_i}^{\infty} \frac{\xi \cdot \varepsilon_{2,\text{TaucLorentz},i}(\xi)}{\xi^2 - En^2} \mathrm{d}\xi. \tag{10}$$

where $\varepsilon_{1,\text{TaucLorentz}}$ and $\varepsilon_{2,\text{TaucLorentz}}$ are the real part and the imaginary part of the TaucLorentz oscillator, respectively. $\varepsilon_{1,\text{TaucLorentz}}$ is derived from $\varepsilon_{2,\text{TaucLorentz}}$ by using the Kramers–Kronig relations [47, 48]. A_i, C_i and E_i stand for the amplitude, the broadening parameter and the position of the $\varepsilon_{2,\text{TaucLorentz},i}$ peak, respectively. Eg_i is the corresponding optical bandgap.

In equations (6)–(10), the fitting coefficients in the dielectric function model including E_∞, E_p, Γ_{Drude}, E_{Lorentz}, A_{Lorentz}, Γ_{Lorentz}, A_1, C_1, E_1, Eg_1, A_2, C_2, E_2 and Eg_2, while N_e, e, m^*, ε_0, τ_{ep}, τ_{ee}, τ_{eb}, τ_{surface} and v_F are regarded as material constants. In our model, the thickness dependency of N_e and τ_{surface} would be discussed thoroughly in the later section. Before the whole-spectrum fitting of ψ_{meas} and Δ_{meas}, the proposed dielectric function model of Cu film has been fitted with the dielectric function of bulk Cu reported by [45] to verify the validity of the dielectric function model, in which a broad spectral range of 0.73–4.96 eV has been covered. The fitting process are carried out via a commercial analysis software (Eometrics, Wuhan Eoptics Technology Co., Wuhan, China). The values of E_∞, E_p, Γ_{Drude}, E_{Lorentz}, A_{Lorentz}, Γ_{Lorentz}, A_1, C_1, E_1, Eg_1, A_2, C_2, E_2 and Eg_2 obtained from such a fitting process will be used as the initial values of the dielectric function in a followed fitting process of ψ_{meas} and Δ_{meas}.

As the thickness of the metallic thin film has been determined through the point-by-point analysis, these coefficients in the dielectric function model can be refined using the whole-spectrum fitting analysis of ψ_{meas} and Δ_{meas}. The

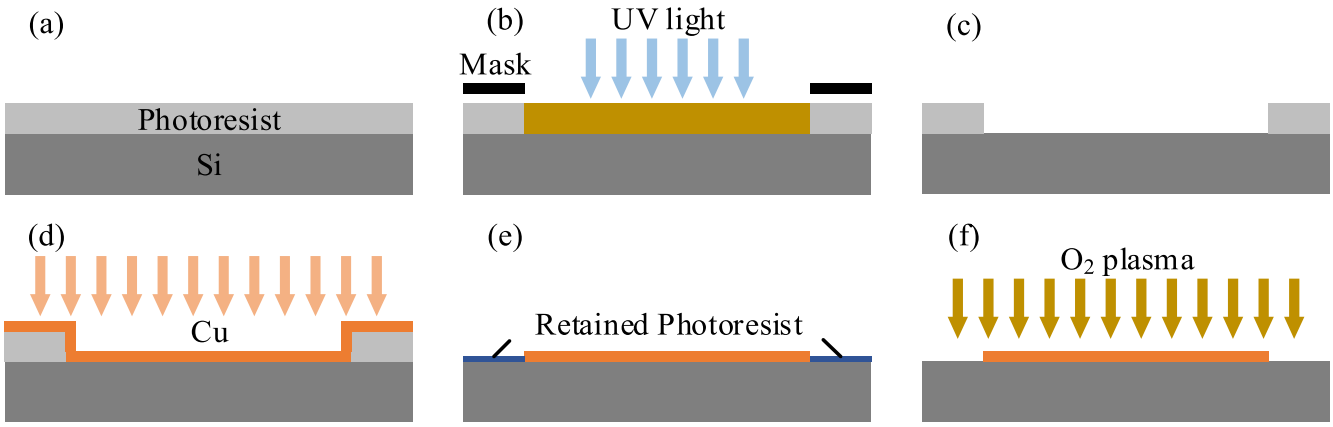

Figure 3. The processing steps of Cu thin films with stairs. (a) spinning, (b) exposing, (c) developing, (d) sputtering Cu film, (e) removing the photoresist, (f) cleaning the retained photoresist by O_2 plasma.

relevant fitting merit function is shown as equation (11),

$$\chi^2 = \frac{1}{2N - M}\sum_{i=1}^{N}\left[\left(\frac{\psi_i^{\text{meas}} - \psi_i^{\text{calc}}}{\sigma(\psi_i^{\text{meas}})}\right)^2 + \left(\frac{\Delta_i^{\text{meas}} - \Delta_i^{\text{calc}}}{\sigma(\Delta_i^{\text{meas}})}\right)^2\right]. \tag{11}$$

where N and M are the total number of wavelength points and the extracted coefficients, respectively.

3. Experiments

In order to adequately verify the validity and the accuracy of the proposed method, experiments on a series of Cu thin films deposited on Si substrates have been carried out.

3.1. Samples preparation

In the experiments, the Cu thin films were sputtered on the Si substrates from the Cu target with purity of 99.999% by using a magnetron sputtering coating system (TPR-450, China) with the mode of DC-sputtering. The sputtering chamber was vacuumed to 5×10^{-3} Pa to drive out the oxygen and water vapor. The sputtering was carried out in Ar (99.99% purity) plasma under a working pressure of 0.3Pa at 300K. Before sputtering, a pre-sputtering process was introduced to remove oxides or other organic impurities from the surface of Cu target. The distance between the target and Si substrate is 35 cm during the sputtering. Before the sputtering, the Si substrate was firstly ultrasonically cleaned by acetone and ethanol for 5 min, respectively. Then the substrate was rained with deionized water and dried with nitrogen flow. Due to the fairly low sputtering power of 50 W, the growth rate of Cu films is less than 0.4 nm s^{-1}. Thus the film surface is smooth so that the roughness can be ignored, where the smooth interface assumption can be supported by the TEM results shown in the next section. By setting different sputtering time, a series of the Cu thin films with different thicknesses were deposited on the Si substrates. The sputtering time and the nominal thickness of each Cu film were given in table 1. After sputtering process, these samples will be immediately measured to minimize the effects of natural oxidation.

Table 1. The sputtering time and nominal thickness of Cu films.

Sputtering time	10 s	20 s	30 s	40 s	50 s	60 s
Nominal thickness	4 nm	6 nm	8 nm	10 nm	12 nm	14 nm

At the same time, reference samples with stairs were fabricated using DC-sputtering combined with lithography, which enables the accurate thickness determination using AFM. The corresponding preparation procedures were shown in figure 3. Firstly, the AZ-5214 photoresist was spun on the Si substrate by a spin coater operating at 4000 rpm for 60 s. Then, the rectangle pattern was constructed by exposing under a mask, and the photoresist structure has been obtained by developing in RD6 solution. Subsequently, Cu layers with different thicknesses have been sputtered on the surface by DC-magnetron sputtering operating at the aforementioned processing parameters. With the samples being immersed in the acetone solution, the photoresist was dissolved with a little retained photoresist. After the retained photoresist was removed by the O_2 plasma within several minutes, a well-defined step between Cu layer and Si substrate had been obtained.

3.2. Measurement of XRD, AFM and TEM

Immediately, the x-ray powder diffraction pattern of the Cu film with nominal thickness of 10 nm has been measured by x-ray diffraction meter with Cu $K\alpha$ radiation (PANalytical PW3040-60 MRD), and the result is shown as figure 4. The diffraction pattern for the Cu film has three peaks at 43.34°, 50.48° and 74.17°, corresponding to (111), (200) and (220) of Cu (ICSD-53247), respectively. No diffraction peaks corresponding to the oxide and the hydroxide of copper have been observed in figure 4. However, it is worth to note that it is still possible existing a few copper oxides and hydroxides in the samples due to the dirty base pressure and the impure

Table 2. Comparison of the measured Cu films using different methods.

Sputtering time		10 s	20 s	30 s	40 s	50 s	60 s
Results achieved by method	Thickness d_m (nm)	3.90 ± 0.06	6.80 ± 0.15	8.70 ± 0.25	9.90 ± 0.10	11.60 ± 0.28	12.90 ± 0.31
	MSE	1.89×10^{-6}	8.62×10^{-6}	1.05×10^{-5}	2.08×10^{-5}	1.29×10^{-5}	8.47×10^{-6}
Thickness achieved by AFM d_A (nm)		2.86	6.72	8.71	10.00	12.00	12.60
Thickness achieved by TEM d_T (nm)		3.20	—	8.20	—	—	11.90
Relative error between results of the proposed method and AFM, $\mid d_m - d_A \mid / d_A$		0.364	0.012	0.001	0.01	0.033	0.024

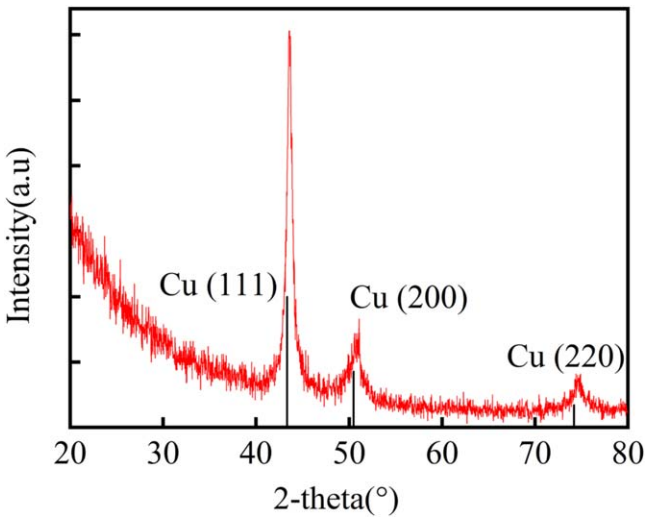

Figure 4. XRD spectra of Cu film with nominal thickness of 10 nm.

argon. Meanwhile the thicknesses of all the Cu films with stairs have been measured by AFM (SPM-9500J3, Shimadzu, Japan), and the results are shown as figures 5(a)–(f). Since the lithography procedures has never damaged the native oxide layer on the original Si substrate, the heights of stairs measured by AFM represent the thicknesses of Cu film layers. Meanwhile, the thicknesses of Cu films with sputtering time of 10, 30 and 60 s have been also measured by TEM (Tecnai F20, Thermo Fisher, USA), and the results are shown as figures 5(g)–(i). Correspondingly, the thicknesses measured by AFM and TEM have also been listed in table 2 for comparison.

3.3. Ellipsometry and reflectometry

After the deposition processes, ψ_{meas}, Δ_{meas} and R_{meas} of these Cu films have been immediately measured by a commercial SE (ME-L, Wuhan Eoptics Technology Co., Wuhan, China) in a wide spectral range from 0.73–4.96 eV under the incident angles of 60°, 65° and 70°. The original Si substrate without Cu covered was also been measured by SE to identify the thickness of the native oxide layer, which has been determined as 1.79 nm and will be used as an input parameter in the experiment.

The point-by-poNint fitting program is self-implemented software using MATLAB, whose flow chart is shown in figure 2. The whole-spectrum fitting program is carried out via a commercial analysis software (Eometrics, Wuhan Eoptics Technology Co., Wuhan, China).

4. Results and discussion

After the measurement of the ellipsometric parameters and the reflectivities of Cu films, the point-by-point fittings of ψ_{meas}, Δ_{meas} and R_{meas} have been implemented and the corresponding thickness of Cu films are determined. The fitting results of Cu film with sputtering time of 40 s under the three incident angles are exhibited in figure 6. We find that both ψ_{meas} and Δ_{meas} are well fitted with the values calculated using the forward optical model. As for R_{meas}, although there exists slight deviations less than 0.01 between R_{meas} and R_{calc}, all the line shapes of the three R_{meas} spectrum are well fitted. It is worth to note that the changes of incident angles introduce no conspicuous deviations in the fitting results of ψ_{meas}, Δ_{meas} and R_{meas}. Therefore, in the rest part of this paper, the regression analysis on ψ_{meas}, Δ_{meas} and R_{meas} measured at the incident angle of 60° is only discussed.

Figure 7 shows the fitting results of the Cu films with different thicknesses under the incident angle of 60°. Similar to the results presented in figure 6, both ψ_{meas} and Δ_{meas} of each Cu film have been well fitted with the calculated ones. And R_{meas} of each Cu film is also fitted well with small fitting deviation less than 0.01. Considering that these Cu films has been measured for three times, the average thickness, the standard deviations of thickness and the total MSE are determined and listed in table 2. It should be noted that all the values are the effective thicknesses of Cu films due to the possible rough or oxide layer on the Cu films. However, due to the low sputtering power and the short exposure time in air between fabrication and measurement, the roughness and oxidation effects can be ignored.

Meanwhile, point-by-point fittings of the single-angle ψ_{meas} and Δ_{meas} and the multi-angle ψ_{meas} and Δ_{meas} combining with R_{meas} or without R_{meas} have also been carried out to extract the thicknesses of Cu films. Correspondingly, the total MSE curves achieved on the Cu film with sputtering time of 40 s are exhibited in figure 8. The results shown in figure 8 indicate that the uniqueness of the fitting results extracted using the proposed method is remarkably better than the ones extracted using other fitting methods, which reflects the optimal sensitivity and robustness of the proposed method. As shown by the blue dash line in figure 8(a),

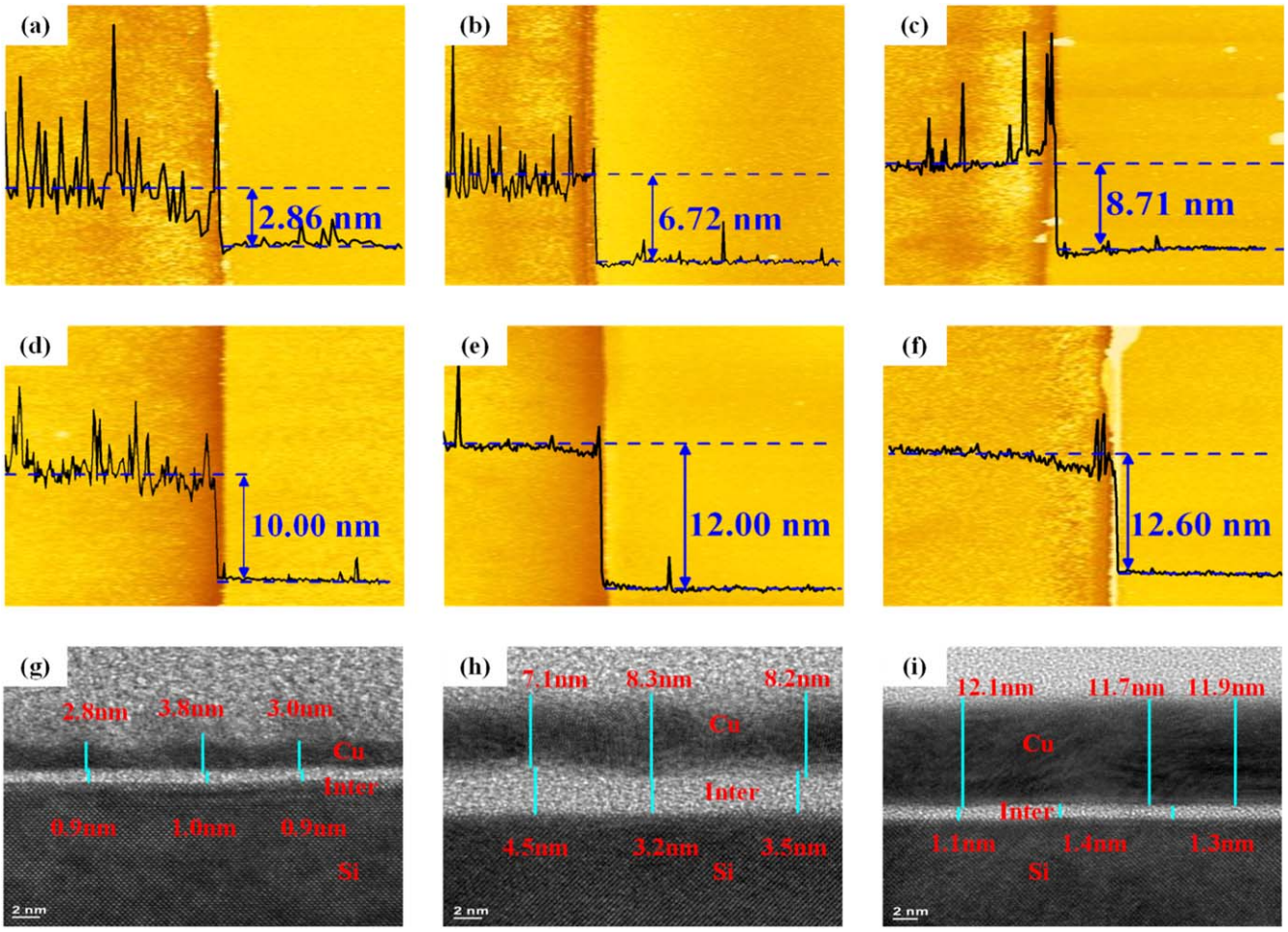

Figure 5. The results of the Cu films measured by AFM and TEM. (a)–(f) The results of the Cu thin films with sputtering time of 10–60 s measured by AFM. (g)–(i) The results of the Cu thin films with sputtering time of 10, 30 and 60 s measured by TEM.

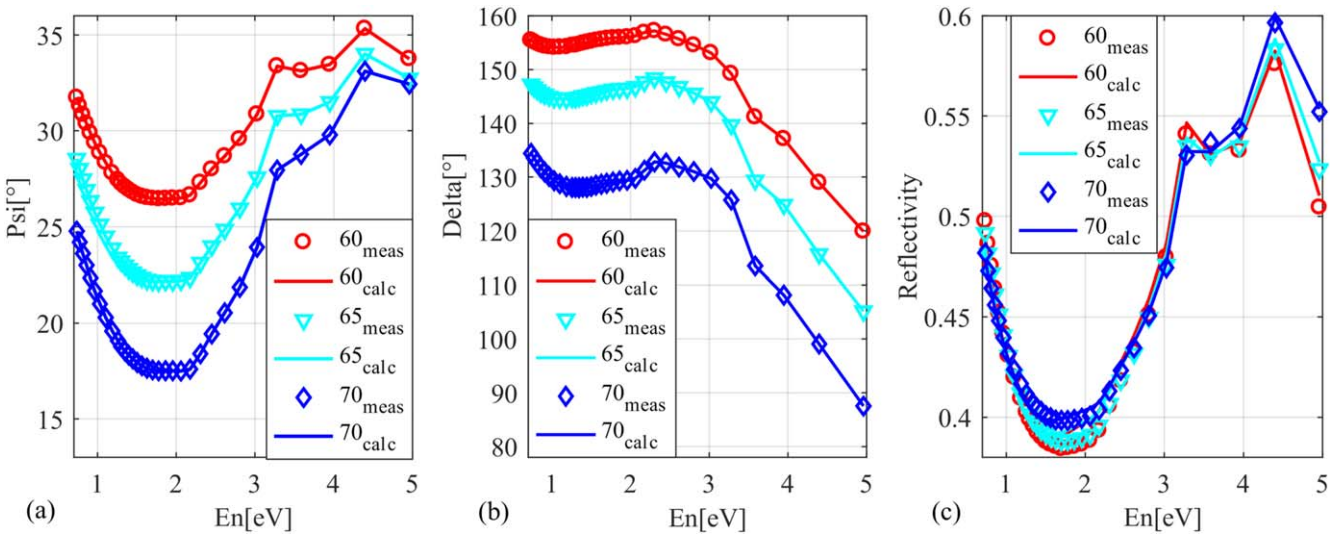

Figure 6. Synergic fitting results of the Cu film with sputtering time of 40 s. (a) Fitting results of ψ_{meas} under $\theta = 60°$, 65° and 70°, (b) fitting results of Δ_{meas} under $\theta = 60°$, 65° and 70°, (c) fitting results of R_{meas} under $\theta = 60°$, 65° and 70°.

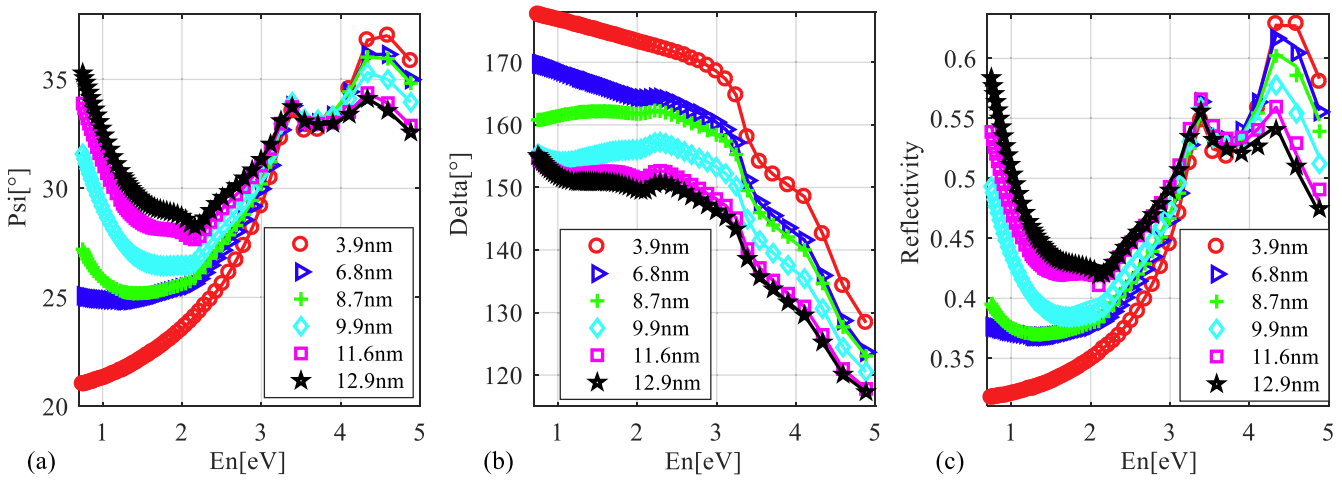

Figure 7. Synchronous fitting results of ψ_{meas}, Δ_{meas} and R_{meas} of all the Cu films under an incident angle of 60°. (a) Fitting results of ψ_{meas} for each Cu thin films under $\theta = 60°$, (b) fitting results of Δ_{meas} for each Cu thin films under $\theta = 60°$, (c) fitting results of R_{meas} for each Cu thin films under $\theta = 60°$.

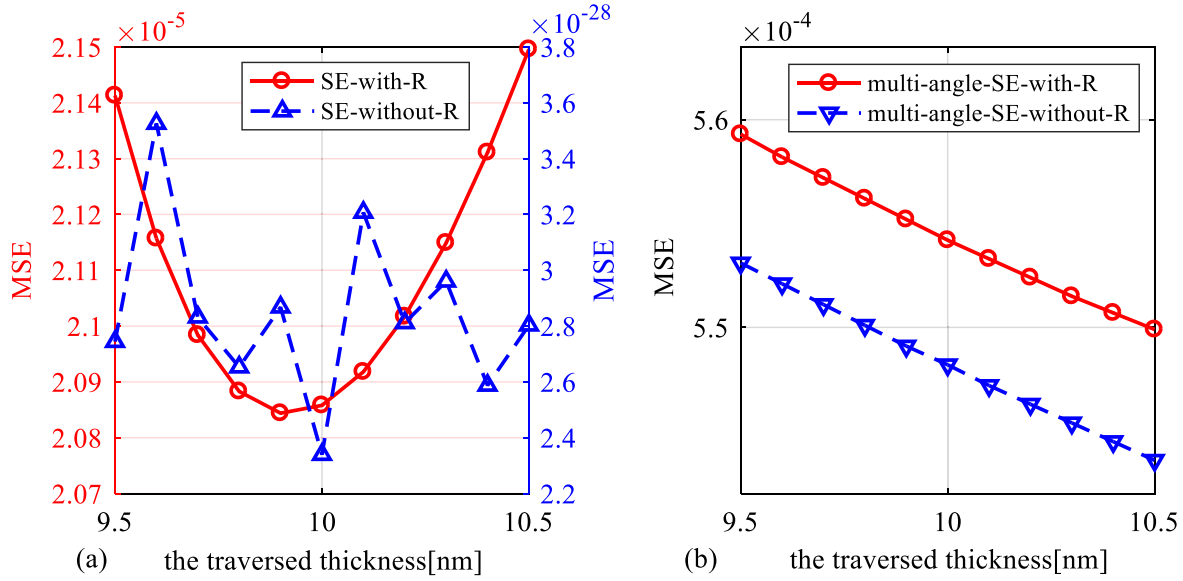

Figure 8. Sensitivity analysis for different methods. (a) Red line corresponds to the results obtained using the proposed method, while blue line corresponds to the results obtained only using ellipsometric parameters. (b) Red solid line corresponds to the results obtained by one-step regression using multi-angle ellipsometric parameters and reflectivities, blue solid line corresponds to the results obtained by one-step regression using multi-angle ellipsometric parameters only.

although the MSE achieved by fitting the single-angle ψ_{meas} and Δ_{meas} without reflectivity input is extremely small, the method is insensitive to extracting the thickness. Meanwhile, the results in figure 8(b) show that no unique solution of thickness can be achieved by multi-angle data no matter if the reflectivity is used. Such phenomena can be attributed to the large fitting errors of multi-angle ψ_{meas} and Δ_{meas} or the possible inappropriate selection of incident angle combination. In Fact, the uniqueness of the fitting results for all the film samples obtained by the proposed method is noticeably better than the ones obtained using other fitting methods, which highlights the necessity and worth of the proposed method.

As shown in table 2, the measured thicknesses reported by the proposed method, AFM and TEM are in a good agreement. It is worthy of noting that inconspicuous oxide layers on the Cu films have been observed in figures 5(g)–(i) and the Cu films observed in figures 5(b)–(f) are rather smooth, which identify the validity of neglecting the roughness and oxidation effects on the Cu films in the previous discussions. It has been noticed that the results on the sample with the sputtering time of 10 s reported by AFM and the proposed method have relative error larger than 30%. It might be due to the isolated island structure in the surface of Cu film with a such short sputtering time. In fact, with the sputtering time increasing, the Cu film will be gradually formed from the

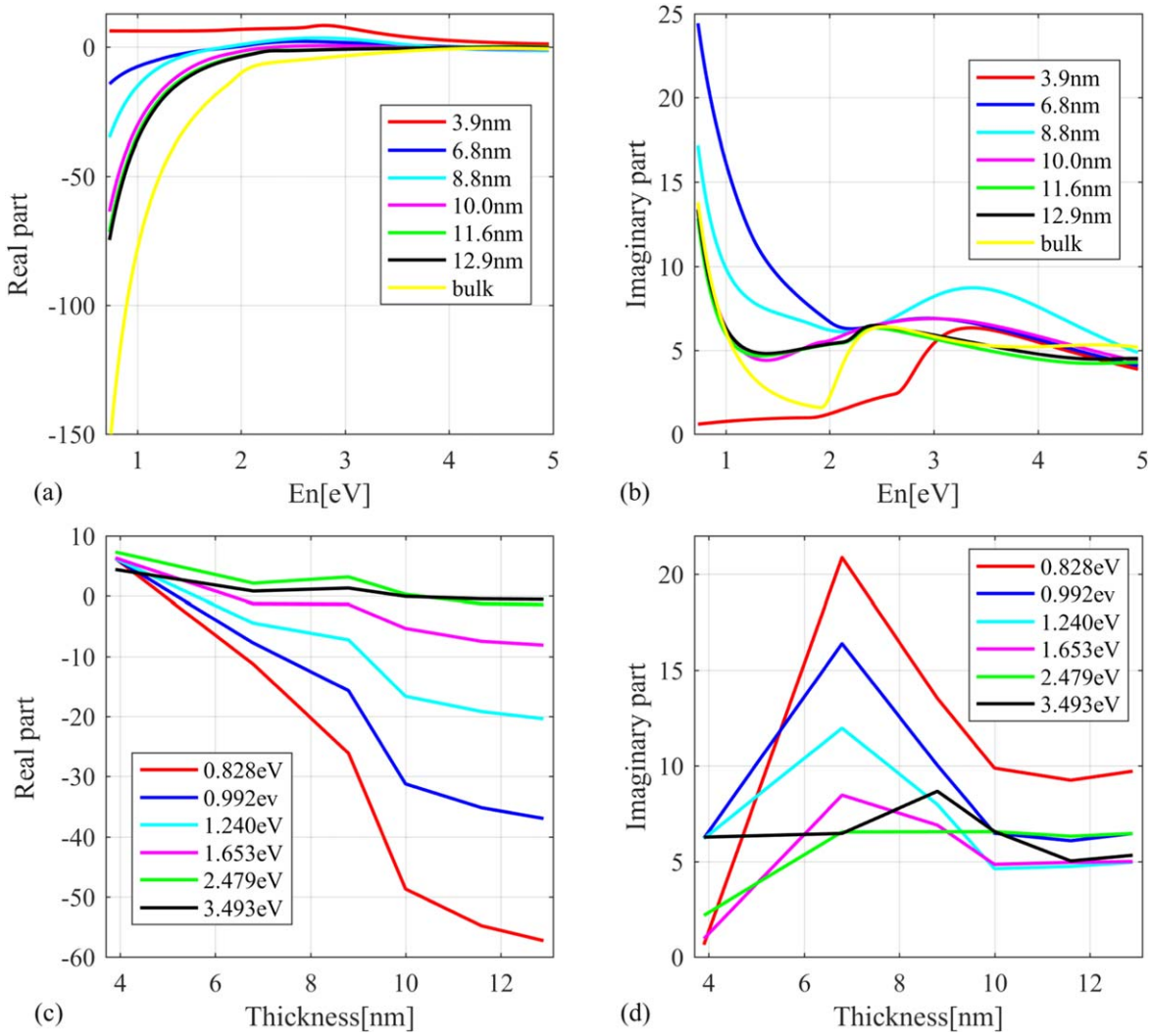

Figure 9. Dielectric function of the Cu films: (a) real part; (b) imaginary part; (c) real part at special energy point; (d) imaginary part at special energy point.

granular film to the continuous film according to the results in figure 5. Namely, the first Cu film shown in figure 5(a) is distributed with isolated islands, and the Cu films shown in figures 5(b)–(f) are continuous and flat. The former may be due to the low mobility of adatom caused by the residual stress in the interface between Cu film and Si substrate [49]. And the latter can be attributed to the coalescence of islands and the channel filling due to the increasing mobility of the deposited Cu atoms [50]. It is worth to mention that ψ_{meas}, Δ_{meas} and R_{meas} of Cu film with thickness of 3.9 nm are remarkably similar to that of Si substrate [20]. Meanwhile, these parameters of Cu films with larger thickness are distinctly different from that of Si substrate. It indicates that ψ_{meas}, Δ_{meas} and R_{meas} of the ultrathin film can be primarily attributed to the optical properties of Si substrate, which could be an evidence showing the partial covering status of the Cu layer on Si substrate. In addition, it further shows that the percolation threshold of Cu film is between 3.9 and 6.8 nm, which is similar to the corresponding value of Au [42]. Correspondingly, the thickness of 3.9 nm measured by SE is only a roughly equivalent value from the point-by-point fitting. In addition, the results in figure 5(g) indicated that the Cu film is indeed uncontinuous and the maximum thickness of 3.8 nm can be clearly observed by TEM. Moreover, all the absolute deviations between the thicknesses measured by the proposed method and by AFM or TEM are less than 1 nm. The consistent results show that the smooth surface assumption is valid. Meanwhile, the results of multi-point measurement have also verified this assumption. Besides, the results of Energy Dispersive x-ray spectroscopy measurement for Cu film with thickness of 3.9 nm, companied with TEM, shows that the ratio of the mass fraction of oxygen to copper on the surface of Cu film is less than $1/16$. The result implies that the surface oxidation can be omitted in the analysis of thickness. As for the fluctuation of dielectric properties of Silicon dioxide in lateral direction, the effect could be omitted according to the results reported by [20]. The fluctuation of dielectric functions is usually caused by the thickness fluctuation of Silicon dioxide. The thickness fluctuations of Silicon dioxide in our Cu films are less than 0.1–0.3 nm.

Table 3. Fitting coefficients in the dielectric function model for Cu films.

Film thickness (nm)	3.9	6.8	8.7	9.9	11.6	12.9
MSE	1.455	2.305	3.054	2.569	3.399	2.947
E_∞	2.707	1.765	1.795	1.924	2.199	2.041
E_p (eV)	2.714	4.585	5.168	6.374	6.652	6.792
Γ_{Drude} (eV)	11.68	0.455	0.214	0.140	0.118	0.117
$E_{Lorentz}$ (eV)	5.955	5.132	5.201	5.176	0.666	0.912
$A_{Lorentz}$	1.773	1.229	1.459	0.678	3.477	3.967
$\Gamma_{Lorentz}$ (eV)	1.206	1.190	1.420	0.729	0.062	0.758
A_1	3.577	39.72	39.73	55.28	58.99	145.48
C_1 (eV)	0.821	0.356	0.383	0.135	2.139	3.082
E_1 (eV)	3.173	2.248	2.242	2.208	3.274	2.230
Eg_1 (eV)	0.000	2.116	2.119	2.215	1.962	1.994
A_2	5.913	49.965	50.199	52.171	27.567	30.176
C_2 (eV)	1.112	6.738	6.738	5.366	7.710	7.710
E_2 (eV)	3.983	3.182	2.800	3.350	3.194	1.811
Eg_2 (eV)	0.000	0.643	0.714	0.683	0.000	0.329

Thus, the influence of the fluctuation of dielectric properties of Silicon dioxide in lateral direction has been omitted in proposed method.

With the thicknesses of the thin films being determined, the dielectric functions can be extracted by fitting ψ_{meas} and Δ_{meas} based on the proposed parameterized-oscillators model as well. Correspondingly, the fitting coefficients in the dielectric function model are listed in table 3. It is worth to note some irregular changes on the coefficients of the interband transition contributions have been observed, similar to the results reported in [22]. Although the influence of the thickness on the interband transition contributions of dielectric functions is quite complicated and needs further study, the thickness dependences of the coefficients in the intraband transition contributions in table 3 are conspicuous.

Figures 9(a) and (b) show the thickness-dependent real part and the imaginary part of dielectric functions, respectively. Moreover, with the thickness increasing, more and more obvious Drude features of the curves of ε_1 are exhibited, which manifests the stronger metallicity. As for ε_2, the thickness dependency in near-infrared spectral range is more conspicuous. Furthermore, the thickness dependency of the real part and the imaginary part of the dielectric function at some photon energy has also been investigated, as shown in figures 9(c) and (d), respectively. It indicates that at low photon energy, both the real part and the imaginary part of dielectric functions show strong thickness dependency, while at high photon energy, the thickness dependency becomes quite weak. The critical photon energy distinguishing whether the thickness dependency is significant is about 2.478 eV, which is very close to the absorptive peak of bulk Cu due to the first interband transition. These results indicate the unconspicuous thickness dependency of dielectric functions in the high photon energy range might be responsible for the abnormal variation of the coefficients of the interband transition contributions.

Further, we have studied the thickness dependence of the coefficients in the Drude oscillator according to the results in table 3, as shown in figures 10(a) and (b). When the thickness is increasing from 6.8 to 12.9 nm, the plasma energy E_p increases monotonically and the relaxation energy Γ_{Drude} decreases monotonically, which has been observed in [3, 22, 42] as well. According to equation (7.2), the increasing of plasma energy E_p can be attributed to the increasing of N_e/m^*, i.e. the increasing of conduction electron density N_e or the decreasing of electron effective mass m^*. As the Cu films become denser when the thickness increases, the number of Cu atoms per unit volume in the film increases, which means the increasing of the conduction electrons. It is reasonable to attribute the increasing of plasma energy with thickness to the increasing of conduction electron density N_e. The increase of reflectivity with the thickness increase shown in figure 7(c) in the near-infrared range can be attributed to the increase of conduction electron density N_e, which has been reported in literature. Hövel *et al* reported that the decreasing conduction electron density N_e and reflectivity in the Au films when the film thickness is decreasing [42]. Jo de Vries *et al* took the rise of N_e in Ag films as an indicator of the increasing amount of metal [37]. Olmon *et al* has also reported that the voids in the films can cause lower conduction electron density [51]. Although the increasing of plasma energy can also be attributed to the decreasing of electron effective mass m^*, the variation of effective mass m^* is usually interpreted as the variation of conduction electron density N_e [52].

In the early stage of continuous film formation, as the film growth from 6.8 to 10 nm, the increase of the conduction electron density N_e is due to the significant rise in compactness of Cu films. When the thickness of Cu film becomes larger than 10 nm, the increase conduction electron density N_e become slower due to the slower increase in film compactness during continuous film growth. Consequently, a similar increasing trend of the plasma energy as shown in figure 10(a) can be observed. Besides, another possible reason for the irregular increase of plasma energy might be attributed to the presence of little oxygen in the sample, which is not detectable for XRD.

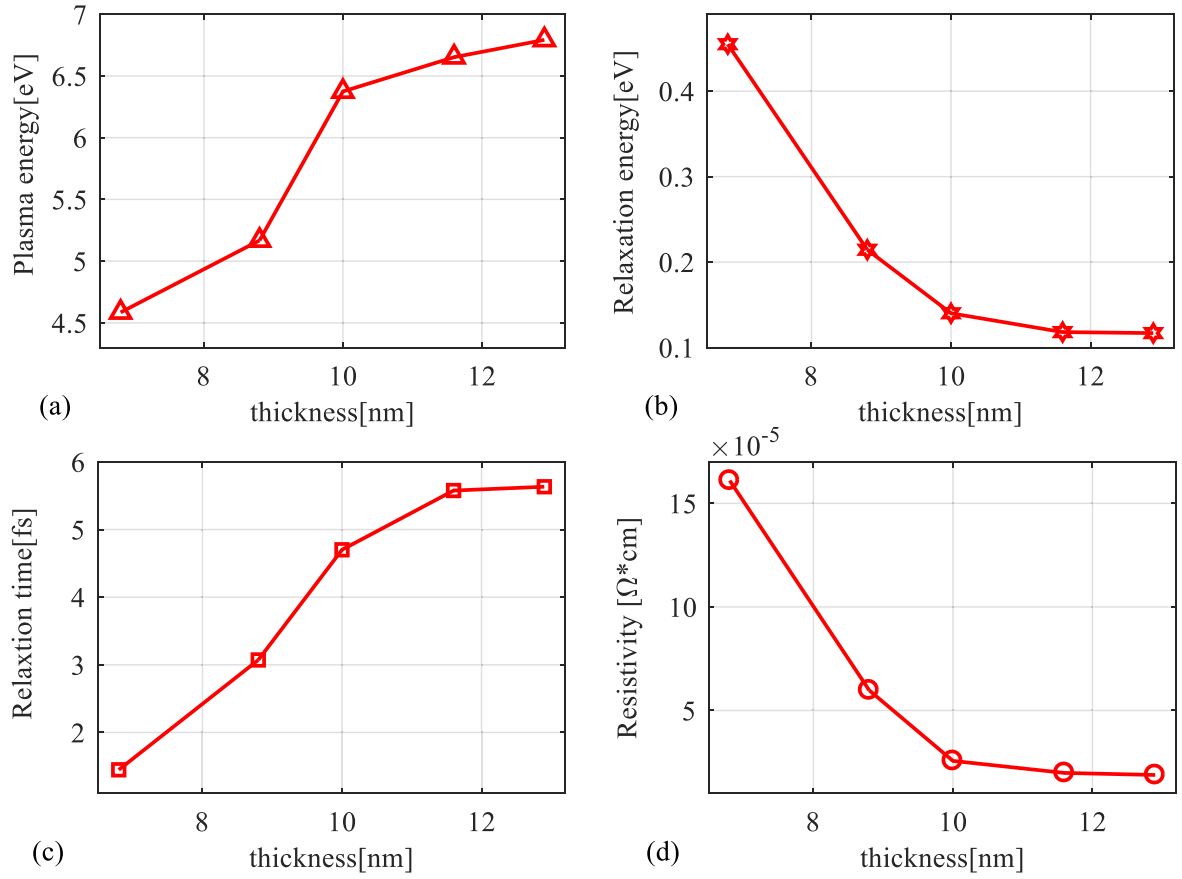

Figure 10. Thickness-dependent optical properties of Cu films with thickness varying from 6.8 to 12.9 nm: (a) plasma energy; (b) electron relaxation energy; (c) electron relaxation time; (d) resistivity.

It is worth noting that the plasma energy of Cu bulk reported in [53] is 8.4 eV, which is slightly larger than the extracted values in our analysis. This indicates the rationality of the thickness dependence of the plasma energy E_p observed in our analysis. Further, the relaxation time $\tau_{Drude} = \hbar/\Gamma_{Drude}$ is increasing with the thickness, as shown in figure 10(c), which evidently indicates the growing metallicity of the Cu films.

Although the sputtered Cu films have been identified as polycrystalline according to the results observed by TEM, no noticeable changes in the grain size of these Cu films are observed. Thus, the thickness dependency of the grain boundary scattering can be negligible. Considering that the electron-phonon scattering, the electron–electron scattering, and the electron-defect scattering are independent of the thickness, τ_{bulk} can be regarded as a constant. Thus, the thickness dependence of τ_{Drude} can be attributed to the thickness dependence of $\tau_{surface}$. By fitting the dielectric function of Cu bulk reported in [45] based on the proposed parameterized-oscillators model, the relaxation time τ_{Drude} can be determined as 10.57 fs. Using the surface relaxation time $\tau_{surface} = 37.51$ fs of Cu bulk reported in [39], the bulk relaxation time τ_{bulk} of Cu bulk can be determined as 14.72 fs. Correspondingly, the surface relaxation time of these Cu thin films can be calculated, as shown in figure 11. The monotonic increasing of the surface relaxation time $\tau_{surface}$ as shown in figure 11 indicates that the surface scattering of conduction electrons has decreased with the thickness increasing.

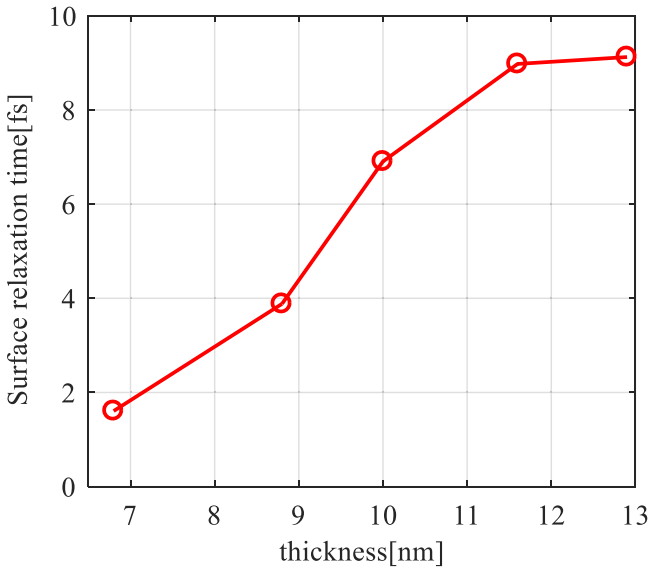

Figure 11. Thickness-dependent surface relaxation time of Cu films, thickness varying from 6.8–12.9 nm.

In addition, the resistivity γ have been calculated from the fitting coefficients in Drude oscillator and shown in

figure 10(d) based on equation (13),

$$\gamma = \frac{\hbar^2}{\varepsilon_0 \tau_{\text{Drude}} E_p^2 e^2}, \tag{13}$$

where $\hbar$, ε_0 and e are the reduced Planck constant, the vacuum dielectric constant and the electron charge, respectively. According to the results shown in figure 10(d), the resistivity is monotonically decreasing with the thickness increasing, which implies the monotonic increasing of the DC conductivity. Thicker films show more and more obvious metallic characteristics.

In above analysis, a comparison between the thicknesses achieved by the proposed method and the ones reported by AFM and TEM has been firstly carried out, and the relative deviations is less than 3.5%, which can be regarded as a demonstration on the accuracy of the thickness measurement of the proposed method. Then, the dielectric functions of Cu films obtained from our method have been compared with the dielectric function of bulk Cu qualitatively, and the variation trend of thickness-dependent dielectric functions of Cu films achieved is rational. Some electronic parameters such as the plasma frequency, the relaxation time and the DC resistivity obtained from the dielectric functions have also been compared with the parameters of bulk Cu, and their variations to the thickness changes are also reasonable. These results indicate the dielectric functions measured by our method are reliable. More importantly, the proposed method has successfully decoupled the strong correlation between the thickness and the dielectric function of metallic thin film, with the outputs of the accurate thickness comparable to the results reported by AFM and TEM and the reliable dielectric functions of Cu thin films in one measurement.

5. Conclusions

In summary, we propose a synergic method based on ellipsometric parameters and reflectivity in a broad spectral range of 0.73–4.96 eV, which enables the simultaneous accurate determination of the thickness and the dielectric function for the metallic thin film using one SE. The proposed method consists of a point-by-point synergic regression analysis on the ellipsometric parameters and the reflectivity as well as an oscillator-parametrization regression analysis on the ellipsometric parameters. A Drude oscillator, two TaucLorentz oscillators and a Lorentz oscillator are used to describe the intraband, the interband and the plasmon contributions to the dielectric functions, respectively. In comparison with the one-step regression method based on multi-angle ellipsometry, the proposed method exhibits improvements in sensitivity and robustness in determining uniqueness solutions. Comparing to a series measurement results reported by AFM and TEM on copper thin films with different thickness, the relative bias of thin film thickness achieved by the proposed are less than 3.5%, which verifies the validity and the accuracy of the proposed method. We also found that both the real part ε_1 and the imaginary part ε_2 of the dielectric functions decrease with the increasing Cu film thickness in the range of 6.8–12.9 nm, while both the plasma energy and the Drude relaxation time increase monotonically with the increasing film thickness. These rational phenomena observed demonstrate the proposed method as well.

Acknowledgments

This work was funded by the National Natural Science Foundation of China (Grant No. 51575214, 51525502, 51727809, and 51805193); the National Key Research and Development Plan (Grant No. 2017YFF0204705); the Natural Science Foundation of Hubei Province of China (Grant No. 2018CFA057); and the National Science and Technology Major Project of China (Grant No. 2017ZX02101006-004); the China Postdoctoral Science Foundation (Grant Nos. 2016M602288 and 2017T100546).

ORCID iDs

Hao Jiang https://orcid.org/0000-0003-0561-5058
Xiuguo Chen https://orcid.org/0000-0002-7067-5084
Guanglan Liao https://orcid.org/0000-0002-1849-5473
Shiyuan Liu https://orcid.org/0000-0002-0756-1439

References

[1] Liu N, Mesch M, Weiss T, Hentschel M and Giessen H 2010 Infrared perfect absorber and its application as plasmonic sensor *Nano Lett.* **10** 2342–8
[2] Xu J P, Zhang R J, Zhang Y, Wang Z Y, Chen L, Huang Q H, Lu H L, Wang S Y, Zheng Y X and Chen L Y 2016 The thickness-dependent band gap and defect features of ultrathin ZrO_2 films studied by spectroscpic ellipsometry *Phys. Chem. Chem. Phys.* **18** 3316–21
[3] Gong J B, Dai R C, Wang Z P and Zhang Z M 2015 Thickness dispersion of surface plasmon of Ag nano-thin films: determination by ellipsometry iterated with transmittance method *Sci. Rep.* **5** 9297
[4] Yakubovsky D I, Arsenin A V, Stebunov Y V, Fedyanin D Y and Volkov V S 2017 Optical constants and structural properties of thin gold films *Opt. Express* **25** 25574–87
[5] Özer M M, Jia Y, Zhang Z Y, Thompson J R and Weitering H H 2007 Tuning the quantum stability and superconductivity of ultrathin metal alloys *Science* **316** 1594–7
[6] Wong C L and Olivo M 2014 Surface plasmon resonance imaging sensors: a review *Plasmonics* **9** 809–24
[7] Ahn J H and Kwon S H 2015 Sub-0.5 nm equivalent oxide thickness scaling for Si-doped $Zr_{1-x}Hf_xO_2$ thin film without using noble metal electrode *ACS Appl. Mater. Interfaces* **7** 15587–92
[8] Tompkins H G, Zhu T and Chen E 1998 Determining thickness of thin metal films with spectroscopic ellipsometry for applications in magnetic random-access memory *J. Vac. Sci. Technol.* A **16** 1297–302
[9] Kildishev A V, Boltasseva A and Shalaev V M 2013 Planar photonics with metasurfaces *Science* **339** 1232009

[10] Sergeant N P, Agrawal M and Peumans P 2010 High performance solar-selective absorbers using coated sub-wavelength gratings *Opt. Express* **18** 5525–40

[11] Synowicki R A 1998 Spectroscopic ellipsometry characterization of indium tin oxide film microstructure and optical constants *Thin Solid Films* **313–314** 394–7

[12] Liu C, Erdmann J, Maj J and Macrander A 1999 Thickness determination of metal thin films with spectroscopic ellipsometry for x-ray mirror and multilayer applications *J. Vac. Sci. Technol.* A **17** 2714–48

[13] Oates T W H, Ryves L and Bilek M M M 2008 *Opt. Express* **16** 2302–14

[14] Zhang M Y, Wang Z Y, Zhang T N, Zhang Y, Zhang R J, Chen X, Sun Y, Zheng Y X, Wang S Y and Chen L Y 2016 Thickness-dependent free-electron relaxation time of Au thin films in near-infrared region *J. Nanophoton* **10** 033009

[15] Hilfiker J N, Singh N, Tiwald T, Convey D, Smith S M, Baker J H and Tompkins H G 2008 Survey of methods to characterize thin absorbing films with spectroscopic ellipsometry *Thin Solid Films* **516** 7979–89

[16] Urban F K III, Barton D and Tiwald T 2009 Numerical ellipsometry: analysis of thin metal layers using n-k plane methods with multiple incidence angles *Thin Solid Films* **518** 1411–4

[17] McGahan W A, Johs B and Woollam J A 1993 Techniques for ellipsometric measurement of the thickness and optical constants of thin absorbing films *Thin Solid Films* **234** 443–6

[18] Langereis E, Heil S B S, van de Sanden M C M and Kessels W M M 2006 *In situ* spectroscopic ellipsometry study on the growth of ultrathin TiN films by plasma-assisted atomic layer deposition *J. Appl. Phys.* **100** 023534

[19] Tompkins H G and Tasic S 2000 Synergism of transmission measurements with spectroscopic ellipsometry measurements in the analysis of a nearly opaque bimetal film stack on glass *J. Vac. Sci. Technol.* A **18** 946–50

[20] Herzinger C M, Johs B, McGahan W A, Woollam J A and Paulson W 1998 Ellipsometric determination of optical constants for silicon and thermally grown silicon dioxide via a multi-sample, multi-wavelength, multi-angle investigation *J. Appl. Phys.* **83** 3323–36

[21] Liang X N, Xu X W, Zheng R T, Abel Lum Z M and Qiu J J 2015 Optical constant of CoFeB thin film measured with the interference enhancement method *Appl. Opt.* **54** 1557–63

[22] Hu E T, Cai Q Y, Zhang R J, Wei Y F, Zhou W C, Wang S Y, Zheng Y X, Wei W and Chen L Y 2016 Effective method to study the thickness-dependent dielectric functions of nanometal thin film *Opt. Lett.* **41** 4907–10

[23] Tompkins H G and Hilfiker J N 2016 *Spectroscopic Ellipsometry Practical Application to Thin Film Characterization* (New York: Momentum Press)

[24] Li J, Tang J Y, Pei W, Wei X H and Huang F 2015 Accurate determination of thickness values and optical constants of absorbing thin films on opaque substrates with spectroscopic ellipsometry *Acta Phys. Sin.* **64** 110702

[25] Philipp L, Michael S, Bjoern N, Jeremie W, Miha F, Soo-Jin M, Jun-Ho Y, Marko T, Stefaan D W and Christophe B 2015 Complex refractive index spectra of $CH_3NH_3PbI_3$ perovskite thin films determined by spectroscopic ellipsometry and spectrophotometry *J. Phys. Chem. Lett.* **6** 66–71

[26] Pribil G K, Johs B and Ianno N J 2004 Dielectric function of thin metal films by combined *in situ* transmission ellipsometry and intensity measurements *Thin Solid Films* **455–456** 443–9

[27] Lizana A, Foldyna M, Stchakovsky M, Georges B, Nicolas D and Garcia C B 2013 Enhanced sensitivity to dielectric function and thickness of absorbing thin films by combining total internal reflection ellipsometry with standard ellipsometry and reflectometry *J. Phys. D: Appl. Phys.* **46** 105501

[28] Hans A, Michal P and Knut J 2004 Total internal reflection ellipsometry principles and applications *Appl. Opt.* **43** 3028–36

[29] McIntyre J D E and Aspnes D E 1971 Differential reflection spectroscopy of very thin surface films *Surf. Sci.* **24** 417–34

[30] Tompkins H G and Irene E A 2005 *Handbook of Ellipsometry* (New York: William Andrew, Inc) pp 76–80

[31] Xie D, Qiu Z, Wang L, Talwar D, Cheng H, Liu S, Mei T and Feng Z 2017 Spectroscopic ellipsometry and x-ray diffraction studies on $Si_{1-x}Ge_x$/Si epifilms and superlattices *Appl. Surf. Sci.* **421** 748–54

[32] Oates T W H, Wormeester H and Arwin H 2011 Characterization of plasmonic effects in thin films and metamaterials using spectroscopic ellipsometry *Prog. Surf. Sci.* **86** 328–76

[33] Zhang C, Liu S, Shi T and Tang Z 2011 Fitting-determined formulation of effective medium approximation for 3D trench structures in model-based infrared reflectrometry *J. Opt. Soc. Am.* A **28** 263–71

[34] Reuter G E H and Sondheimer E H 1948 The theory of the anomalous skin effect in metals *Proc. R. Soc. A-Math. Phys.* **195** 336–64

[35] Larkin I A, Keil K, Vagov A, Croitoru M D and Axt V M 2017 Superanomalous skin effect for surface plasmon polaritons *Phys. Rev. Lett.* **119** 176801

[36] Chen X, Liu S, Zhang C, Jiang H, Ma Z, Sun T and Xu Z 2014 Accurate characterization of nanoimprinted resist patterns using Mueller matrix ellipsometry *Opt. Express* **22** 15165–77

[37] Jo de Vries A, Kooij E S, Wormeester H, Mewe A A and Poelsema B 2007 Ellipsometric study of percolation in electroless deposited silver films *J. Appl. Phys.* **101** 053703

[38] Harsha R, Urcan G, Krishnakali C, Aveek D, Alexander V K, Vladimir M S and Alexandra B 2017 Temperature-dependent optical properties of single crystalline and polycrystalline silver thin films *ACS Photonics* **4** 1083–91

[39] Xu M, Yang J Y, Zhang S Y and Liu L H 2017 Role of electron-phonon coupling in finite-temperature dielectric functions of Au, Ag, and Cu *Phys. Rev.* B **96** 115154

[40] Beach R T and Christy R W 1977 Electron-electron scattering in the intraband optical conductivity of Cu, Ag and Au *Phys. Rev.* B **16** 5277–84

[41] Ashcroft N and Sturm K 1971 Interband absorption and the optical properties of polyvalent metals *Phys. Rev.* B **3** 1898–910

[42] Hövel M, Gompf B and Dressel M 2010 Dielectric properties of ultrathin metal films around the precolation threshold *Phys. Rev.* B **81** 035402

[43] Rakić A D, Djurišić A B, Elazar J M and Majewski M L 1998 Optical properties of metallic films for vertical-cavity optoelectronic devices *Appl. Opt.* **37** 5271–83

[44] Etchegoin P G, Le R E C and Meyer M 2006 An analytic model for the optical properties of gold *J. Chem. Phys.* **125** 164705

[45] Palik E D 1998 *Handbook of Optical Constants of Solids* (New York: Academic) 280–6

[46] Fujiwara H 2007 *Spectroscopic Ellipsometry Principles and Applications* (New York: Wiley) 170–2

[47] Jellison G E Jr and Modine F A 1996 Parameterization of the optical functions of amorphous materials in the interband region *Appl. Phys. Lett.* **69** 371–3

[48] Jellison G E Jr and Modine F A 1998 Erraum: parameterization of the optical functions of amorphous materials in the interband region *Appl. Phys. Lett.* **69** 2137

[49] Friesen C, Seel S C and Thompson C V 2004 Reversible stress changes at all stage of Volmer-Weber film growth *J. Appl. Phys.* **95** 1011–20

[50] Oates T W H, Ryves L and Bilek M M M 2007 Dynamic spectroscopic ellipsometry determination of nanostructural changes in plasmonic silver films *Opt. Express* **15** 15987–98

[51] Olmon R L, Slovick B, Johnson T W, Shelton D, Oh S H, Boreman G D and Raschke M B 2012 Optical dielectric function of gold *Phys. Rev.* B **86** 235147

[52] Theye M L 1970 Investigation of the optical properties of Au by means of thin semitransparent films *Phys. Rev.* B **2** 3060–78

[53] Ordal M A, Long L L, Bell R J, Bell S E, Bell R R, Alexander R W and Ward C A 1983 Optical properties of the metals Al, Co, Cu, Au, Fe, Pb, Ni, Pd, Pt, Ag, Ti, and W in the infrared and far infrared *Appl. Opt.* **22** 1099–119